Coherent Manipulation of Electronic States in a Double Quantum Dot

T. Hayashi,[1] T. Fujisawa,[1] H. D. Cheong,[2] Y. H. Jeong,[3] and Y. Hirayama[1,4]

[1]*NTT Basic Research Laboratories, NTT Corporation, 3-1 Morinosato-Wakamiya, Atsugi, 243-0198, Japan*
[2]*Hanbat National University, Deok Myung Dong Yusung Gu Daejon, Korea*
[3]*Pohang University of Science and Technology, Pohang, Kyungpook, Korea*
[4]*CREST, 4-1-8 Honmachi, Kawaguchi, 331-0012, Japan*
(Received 9 June 2003; published 26 November 2003)

We investigate coherent time evolution of charge states (pseudospin qubit) in a semiconductor double quantum dot. This fully tunable qubit is manipulated with a high-speed voltage pulse that controls the energy and decoherence of the system. Coherent oscillations of the qubit are observed for several combinations of many-body ground and excited states of the quantum dots. Possible decoherence mechanisms in the present device are also discussed.

Initiated by various experiments on atomic systems, studies on coherent dynamics have been extended to small-scale quantum computers [1]. Nanofabrication technology now allows us to design artificial atoms (quantum dots) and molecules (coupled quantum dots), in which atomic (molecular)- like electronic states can be controlled with external voltages [2–4]. Coherent manipulation of the electronic system in quantum dots and a clear understanding of decoherence in practical structures are crucial for future applications of quantum nanostructures to quantum information technology.

In this Letter, we describe the coherent manipulation of charge states, in which an excess electron occupies the left dot or the right dot of a double quantum dot (DQD). The coherent oscillations between the two charge states are produced by applying a rectangular voltage pulse to an electrode. Although this scheme is analogous to experiments on a superconducting island [5], our qubit is effectively isolated from the electrodes during the manipulation, while it is influenced by strong decoherence during the initialization due to the coupling with the electrodes. This controlled decoherence provides an efficient initialization scheme.

We consider a DQD consisting of left and right dots connected through an interdot tunneling barrier. The left (right) dot is weakly coupled to the source (drain) electrode via a tunneling barrier [see Fig. 1(a)]. The conductance through the device is strongly influenced by the on-site and interdot Coulomb interactions [6]. In the weak-coupling regime at a small source-drain voltage, V_{sd}, a finite current is only observed at the triple points, where tunneling processes through the three tunneling barriers are allowed. Under an appropriate condition where only the interdot tunneling is allowed, Coulomb interactions effectively isolate the DQD from the source and drain electrodes. In this case, we can consider two charge states, in which an excess electron occupies the left dot ($|L\rangle$) or the right dot ($|R\rangle$) with electrochemical potentials E_L and E_R, respectively. In practice, each charge state involves (many-body) ground and excited

states. When the two specific states are energetically close to each other and the excitation to other states can be neglected, the system can be approximated as a two-level system (qubit). It is characterized by the energy offset, $\varepsilon \equiv E_R - E_L$, and the interdot tunneling, which gives an anticrossing energy, Δ [3]. The effective Hamiltonian is

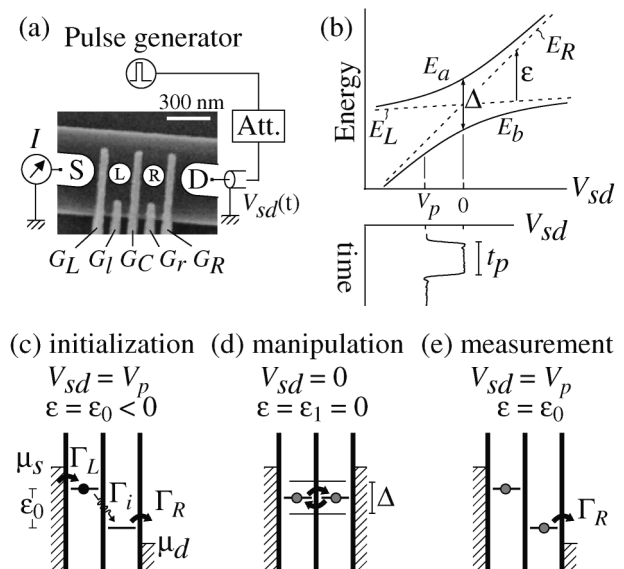$$H = \frac{1}{2}\varepsilon(t)\sigma_z + \frac{1}{2}\Delta\sigma_x, \qquad (1)$$

FIG. 1. (a) Schematic measurement circuit combined with a scanning electron microscope image of the sample. Etching (upper and lower dark regions) and negatively biased gate electrodes (G_L, G_l, G_C, G_r, and G_R) define a double quantum dot (L and R) between the source (S) and drain (D). (b) Energy levels of the bonding (E_b) and antibonding (E_a) states, which are the eigenstates during the manipulation, and localized states (E_L and E_R) during initialization. A typical condition of $\varepsilon_1 = 0$, where E_L and E_R cross at $V_{sd} = 0$, is shown. A typical pulsed voltage $V_{sd}(t)$ is shown at the bottom. (c)–(e) Energy diagrams of the DQD for $\varepsilon_1 = 0$ during (c) initialization, (d) coherent oscillation, and (e) measurement process.

where σ_x and σ_z are the Pauli matrices for pseudospin bases of $|L\rangle$ and $|R\rangle$. When E_L and E_R of the localized states are crossed by changing V_{sd}, for instance, as shown by dashed lines in Fig. 1(b), the eigenenergies, E_b and E_a, for bonding and antibonding states, respectively, show anticrossing as shown by solid lines. The coherent oscillation of the system is expected with the angular frequency given by $\Omega = \sqrt{\varepsilon^2 + \Delta^2}/\hbar$.

The DQDs (samples I and II with almost identical dimensions) used for this work are defined in a GaAs/AlGaAs heterostructure containing a two-dimensional electron gas, as shown in Fig. 1(a). The experiments were performed in a magnetic field of 0.5 T to avoid unwanted degeneracy and at lattice temperature $T_{\text{lat}} \lesssim$ 20 mK, unless otherwise noted. The effective electron temperature, however, remained at $T_{\text{elec}} \sim 100$ mK. Each dot in both samples contains about 25 electrons and has an on-site charging energy $E_c \sim 1.3$ meV. The interdot electrostatic coupling energy is $U \sim 200\ \mu$eV. Figure 2(a) shows the current spectrum I of sample I when the voltage, V_R, on the right gate [G_R in Fig. 1(a)] is swept at a large source-drain voltage $V_{sd} = 650\ \mu$V. Each dot contains several energy states in the transport window of width eV_{sd}, and resonant tunneling between them is clearly resolved as current peaks, two of which

FIG. 2 (color).   (a) Current profile, I vs V_R, at constant $V_{sd} = 650\ \mu$V. Two resonant tunneling peaks, α and β, out of about six peaks in the transport window, are shown. The ground state resonant peak (not shown) is located at about 0.5 mV to the right of peak α. Lorentzian fitting (dashed lines) to peaks α and β gives approximate parameters $\hbar\Gamma_L \sim \hbar\Gamma_R \sim 30\ \mu$eV. (b) Color plot of n_p as a function of V_R and t_p. The horizontal axis is also shown in terms of $\varepsilon_{0,i}$ and $\varepsilon_{1,i}$ for resonance i (α or β). (c) $n_p(t_p)$ at $\varepsilon_1 = 0$ [long-dashed lines in (b)] for the resonance α (solid circles) and β (open circles). Lines are fitted to the data. (d) The coupling energy, Δ, determined from the oscillation frequency, when the gate voltage on G_C is changed. The line is a guide for the eye.

(resonances α and β) are shown in Fig. 2(a). Resonance α (β) is probably associated with the ground state of the left dot and the first (second) excited state of the right dot. In the vicinity of each peak, a two-level system (qubit) can be defined by only taking into account a single discrete state in each dot, $|L\rangle$ and $|R\rangle$. The qubit parameters, ε and Δ, and tunneling rates, Γ_L and Γ_R, respectively, for left and right barriers, can be controlled independently by external gate voltages, and are determined from the elastic current spectra [3,4,6].

In order to manipulate the qubit, a rectangular voltage pulse is applied to the drain electrode. This switches the source-drain bias voltage V_{sd} between $V_p = 650\ \mu$V, at which the tunneling between the DQD and the electrodes is allowed, and zero, at which the DQD is effectively isolated from the electrodes due to Coulomb interactions. At the same time, due to the electrostatic coupling between the QDs and electrodes, the pulse also switches the energy offset between $\varepsilon = \varepsilon_0$ at $V_{sd} = V_p$ and ε_1 at $V_{sd} = 0$ ($\varepsilon_1 - \varepsilon_0 \sim 30\ \mu$eV), as shown for $\varepsilon_1 = 0$ in Fig. 1(b). We designed the pulse sequence for initialization, coherent manipulation, and measurement in the following way.

For initialization, a relatively large source-drain voltage, $V_{sd} = V_p$, is applied under appropriate gate voltages, so that E_L and E_R are in between the electrochemical potentials of the source and drain electrodes, μ_S and μ_D ($\mu_S > E_L, E_R > \mu_D = \mu_S - eV_p$). For example, in the off-resonance condition ($\varepsilon = \varepsilon_0 \lesssim -\Delta$) as shown in Fig. 1(c), electron-phonon interaction provides finite inelastic tunneling, whose rate is Γ_i, between the two states [4]. We adjust Γ_L and Γ_R to make them sufficiently larger than Γ_i so that the current would be limited by the inelastic tunneling between the dots. This sequential tunneling process accumulates an excess electron in the left dot, providing the initial state $|L\rangle$. Note that this initialization works even in the resonance condition ($\varepsilon_0 = 0$) when $\hbar\Gamma_L$ and $\hbar\Gamma_R$ are greater than Δ. Significant decoherence from the dissipative tunneling processes holds the system in the localized state $|L\rangle$ rather than in the delocalized states.

For coherent manipulation, we nonadiabatically change V_{sd} to zero, which shifts the energy offset to $\varepsilon = \varepsilon_1$. A typical energy diagram for $\varepsilon_1 \sim 0$ is shown in Fig. 1(d). In this case, the interdot electrostatic coupling prevents the electron tunneling into and out of the DQD by any first-order tunneling process, and negligible current flows through the DQD. Hence the system is well approximated by Eq. (1). The system prepared in $|L\rangle$ goes back and forth between $|L\rangle$ and $|R\rangle$ coherently. We maintain $V_{sd} = 0$ for the pulse length, $t_p = 80 - 2000$ ps, during which the oscillation continues.

Then, the large bias voltage is restored for the measurement [Fig. 1(e)]. The large tunneling rates ($\hbar\Gamma_L$, $\hbar\Gamma_R > \Delta$) effectively stop the coherent manipulation, and thereby provide a strong measurement. If the system ends up in $|R\rangle$ after the manipulation, the electron tunnels
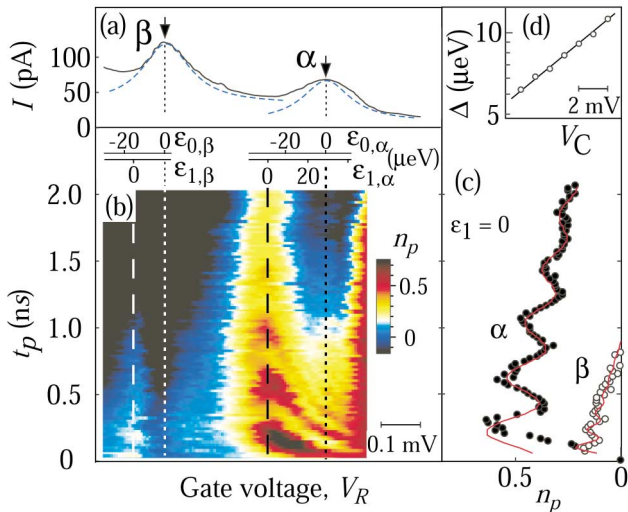
out to the drain electrode and contributes to the pumping current. The system goes back to the initial state $|L\rangle$ after waiting longer than $\Gamma_L^{-1} + \Gamma_R^{-1}$. However, no pumping current is expected for $|L\rangle$, which is already the initial state. Hence, this pumping current depends on the probability of finding the system in $|R\rangle$.

In practice, we repeatedly applied many pulses with a repetition frequency $f_{rep} = 100$ MHz and measured the average dc current, I, which comprises the coherent pumping current and inelastic current that flows during initialization. In order to improve the signal-to-noise ratio, we employed a lock-in amplifier technique to measure the pulse-induced current I_p by switching the pulse train on and off at a low modulation frequency of 100 Hz. We estimated the average number of pulse-induced tunneling electrons, $n_p = I_p/ef_{rep}$.

A color plot of n_p as functions of V_R and t_p is shown in Fig. 2(b). Sweeping V_R mainly shifts E_R and changes the energies ε_0 and ε_1 simultaneously by keeping $\varepsilon_1 - \varepsilon_0$ almost constant. A clear oscillation pattern is observed in a wide range of V_R. Local maxima of the oscillation amplitude appeared for relatively long t_p at gate voltages indicated by long-dashed lines, where the two states must be resonant ($\varepsilon_1 = 0$) during manipulation. We confirmed that the oscillation patterns in Fig. 2(b) are attributed to resonances α (clear oscillation) and β(faint oscillation) from their V_p dependence. The energy offsets $\varepsilon_{0,i}$ and $\varepsilon_{1,i}$ for resonance i (α and β) are also shown in Fig. 2(b).

The oscillation pattern for resonance α shows that the amplitude and period decrease as $\varepsilon_{1,\alpha}$ goes away from $\varepsilon_{1,\alpha} = 0$. The current amplitude is asymmetric about $\varepsilon_{1,\alpha} = 0$, and the oscillation continues until $\varepsilon_{1,\alpha} \sim 40$ μeV. These features are qualitatively consistent with a calculation based on the time-dependent Schrödinger equation and Eq. (1) using a time-dependent $\varepsilon(t)$ with a finite rise time ($\sim$100 ps) of the pulse [5]. It should be noted that clear oscillation is seen even at $\varepsilon_{0,\alpha} = 0$ (indicated by a black dotted line), where two localized states are resonant during the initialization but off-resonant during the manipulation. This feature is convincing evidence that there is strong decoherence during initialization. The density matrix calculation for our initialization condition gives the decoherence rate, $\hbar(\Gamma_R + \Gamma_L)/2 \sim 30$ μeV [7], which is greater than $\Delta = 9$ μeV for resonance α. However, the Coulomb blockade effect eliminates this decoherence during manipulation. Therefore, we presume that the oscillation at $\varepsilon_{0,\alpha} = 0$ is induced by the modulation of the decoherence rate. In contrast, the disappearance of the oscillation at $\varepsilon_{0,\beta} = 0$ (indicated by a white dotted line) for resonance β ($\Delta = 30$ μeV) might arise from the inefficient initialization that provides a statistical mixture of bonding and antibonding states.

The qubit state can be manipulated arbitrarily. Ideally, the quarter period oscillation at $\varepsilon_1 = 0$ corresponds to the $\pi/2$ pulse that prepares a superposition state $\frac{1}{\sqrt{2}}(|L\rangle - i|R\rangle)$. Leaving a state at $\varepsilon = \varepsilon_2 \gg \Delta$ for a specific time

t_ϕ gives a phase shift $\varepsilon_2 t_\phi/\hbar$ between $|L\rangle$ and $|R\rangle$. Therefore arbitrary states can be prepared by tailoring the pulse waveform $\varepsilon(t)$ even at a constant Δ. The demonstration of phase-shift operations will be published elsewhere [8].

Figure 2(c) shows typical $n_p(t_p)$ traces at $\varepsilon_1 = 0$ for resonances α and β. The oscillation can be fitted well by an exponential decay of the cosine function and a linearly decreasing term,

$$n_p(t_p) \simeq A - \frac{1}{2}B\exp(-t_p/T_2)\cos(\Omega t_p) - \Gamma_i t_p, \quad (2)$$

except when $t_p \lesssim 100$ ps (the rise time of the pulse). The last term comes from the fact that the inelastic tunneling current is blocked during the manipulation. Actually $\Gamma_i \sim (6 \text{ ns})^{-1}$ obtained for α from this fitting is consistent with the inelastic dc current, which should be $e\Gamma_i$ in the absence of the pulse. The offset, $A \sim 0.6$, and amplitude, $B \sim 0.3$, of the oscillation for α are comparable to the ideal case ($A = 0.5$ and $B = 1$ at $\varepsilon_1 = 0$), although they are degraded by the finite rise time of the pulse and nonideal initialization/measurement processes. The oscillation frequency Ω and the decoherence time T_2 can be obtained from the fitting ($\Omega/2\pi \sim 2.3$ GHz and $T_2 \sim 1$ ns for resonance α at $\varepsilon_1 = 0$).

We estimate how the decoherence rate T_2^{-1} depends on the energy offset ε_1 [Fig. 3(a)], coupling energy Δ [Fig. 3(b)], and the lattice temperature T_{lat} [Fig. 3(c)]. Here Δ, which is determined from the fitting ($\hbar\Omega$ at $\varepsilon_1 = 0$), can be varied by changing the gate voltage V_C on the
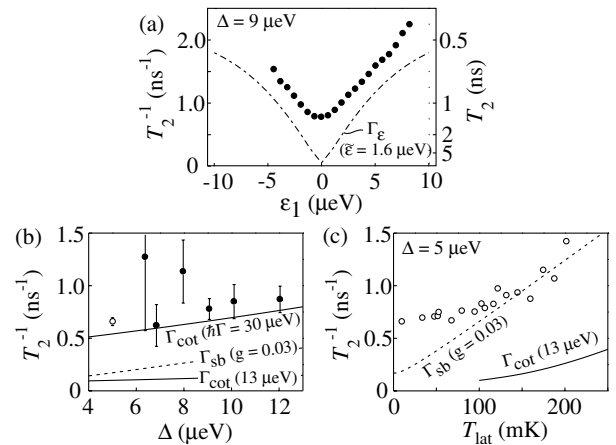

FIG. 3. Decoherence rate, T_2^{-1}, of the qubit. (a) The energy offset (ε_1) dependence. The dash-dotted line shows the decoherence rate, Γ_ε, due to the fluctuation $\tilde{\varepsilon} = 1.6$ μeV. (b) The coupling energy (Δ) dependence. (c) The lattice temperature (T_{lat}) dependence. The solid (open) circles were measured with $\hbar\Gamma_L \sim \hbar\Gamma_R \sim 30$ μeV in sample I ($\hbar\Gamma_L \sim \hbar\Gamma_R \sim 13$ μeV in sample II). The decoherence rates calculated from cotunneling (Γ_{cot}) and spin-boson model (Γ_{sb}) are shown by solid and dashed lines, respectively.

central gate G_C as shown in Fig. 2(d). We discuss some decoherence mechanisms in our measurement.

First, background charge fluctuations and noise in the gate voltages affect ε and Δ, which change the oscillation frequency Ω and dephase the system [9,10]. The fluctuation, $\tilde{\varepsilon}$, of ε in our sample ranges between 1.6 μeV, which is estimated from the fluctuation of I in a frequency range 0.1–5 Hz, and 3 μeV, which is the narrowest linewidth of the resonant peak we obtained in sample I in the weak-coupling limit ($\Delta < 1$ μeV) [4]. The corresponding decoherence rate, $\Gamma_\varepsilon = |d\Omega/d\varepsilon|\tilde{\varepsilon}$ to the lowest order, for $\tilde{\varepsilon} = 1.6$ μeV is shown by a solid line in Fig. 3(a). This qualitatively explains the large decoherence rate at $\varepsilon_1 \neq 0$, where the system is sensitive to $\tilde{\varepsilon}$. However, the decoherence rate at $\varepsilon_1 = 0$ cannot be explained with this model, and should be dominated by other mechanisms.

Second, we consider cotunneling effects. Although the first-order tunneling processes are prohibited during manipulation, higher-order tunneling (cotunneling) processes can occur because relatively high Γ_L and Γ_R were chosen for efficient initialization. For simplicity, we only estimate one of the cotunneling processes, which scatters the electron from the antibonding state to the bonding state (eigenstates of the qubit), from the second order Fermi's golden rule. This gives a transition rate $\Gamma_{\text{cot}} = (8/h)\Delta(\hbar\Gamma)^2/U^2$ at $\varepsilon_1 = 0$, $V_{sd} = 0$ and zero temperature when the barrier is symmetric ($\Gamma = \Gamma_L = \Gamma_R$) [11]. Γ_{cot} shown by solid lines in Figs. 3(b) and 3(c) actually includes thermal broadening in the source and drain [$T_{\text{elec}} = 100$ mK is assumed in Fig. 3(b)]. Although we cannot determine the parameters precisely, Γ_{cot} is comparable to the observed T_2^{-1}. We believe that the cotunneling effect is significant in our measurement but can be easily diminished by choosing smaller Γ and by making the interdot electrostatic coupling energy U larger.

Last, we discuss electron-phonon interactions, which is an intrinsic decoherence mechanism in semiconductor QDs [4,12]. Spontaneous acoustic phonon emission remains even at zero temperature and causes the inelastic tunneling between the two states [4]. The phonon emission rate estimated from the inelastic current or from the fitting with Eq. (2) is $\Gamma_i \sim (4$–20 ns$)^{-1}$, which depends on Δ, at $\varepsilon = -30$ μeV. Γ_i of our interest at $\varepsilon = 0$ should be faster because of the spatial overlap of the eigenstates, and may be comparable to the observed T_2^{-1}. By assuming Ohmic spectral density for simplicity, the spin-boson model predicts the decoherence rate $\Gamma_{sb} = \frac{\pi}{4}g\Delta \coth(\Delta/2k_B T_{\text{lat}})$ for $\varepsilon = 0$. Here the dimensionless coupling constant $g = 0.03$ was chosen to fit with the temperature dependence data for $T_{\text{lat}} > 100$ mK [see dashed line in Fig. 3(c)], and this g is comparable to $g = 0.02$–0.07 used to explain the inelastic current in similar DQD samples [13,14]. Therefore phonon emission should also be significant in our system.

Since many mechanisms dominate the decoherence, we cannot determine each influence quantitatively. However, the qubit is strongly influenced by low-frequency fluctuation when $|\varepsilon| \gtrsim \Delta$, cotunneling at high tunneling rates, and acoustic phonons at high temperature. Moreover, the resonances α and β actually involve excited states in the right dot, and the relaxation to the ground state should also cause decoherence. Other mechanisms, such as the fluctuation of Δ and the electromagnetic environment, may have to be considered to fully understand the decoherence. It should be noted that the quality of the coherent oscillation was improved by reducing high-frequency noise from the gate voltages and the coaxial cable. The remaining noise may also contribute to the decoherence. We hope that some decoherence effects can be reduced by further studies.

In summary, we have successfully manipulated the artificial qubit in a double quantum dot. Coherent oscillations are observed for several combinations of ground and excited states. In the present experiments, there was no condition where two kinds of oscillations coincided, indicating that the two-level system is still a good approximation. However, application of a two-step voltage pulse, which consecutively adjusts the system at two resonances (α and β for instance) in a short time, would mix three quantum states coherently. Therefore, DQDs are promising for studying multilevel coherency [15], and the experiments can be extended to electron-spin manipulations and two-qubit operations [16].

[1] M. A. Nielsen and I. L. Chuang, *Quantum Computation and Quantum Information* (Cambridge Univ. Press, Cambridge, 2000).
[2] S. Tarucha *et al.*, Phys. Rev. Lett. **77**, 3613 (1996).
[3] T. H. Oosterkamp *et al.*, Nature (London) **395**, 873 (1998).
[4] T. Fujisawa *et al.*, Science **282**, 932 (1998).
[5] Y. Nakamura, Yu. A. Pashkin, and J. S. Tsai, Nature (London) **398**, 786 (1999).
[6] W. G. van der Wiel *et al.*, Rev. Mod. Phys. **75**, 1 (2003).
[7] T. H. Stoof and Yu. V. Nazarov, Phys. Rev. B **53**, 1050 (1996).
[8] T. Fujisawa *et al.* (to be published).
[9] T. Itakura and Y. Tokura, Phys. Rev. B **68**, 100405 (2003).
[10] Y. Nakamura *et al.*, Phys. Rev. Lett. **88**, 047901 (2002).
[11] M. Eto, Jpn. J. Appl. Phys. **40**, 1929 (2001).
[12] T. Fujisawa *et al.*, Nature (London) **419**, 278 (2002).
[13] T. Brandes and T. Vorrath, Phys. Rev. B **66**, 075341 (2002).
[14] A. J. Leggett *et al.*, Rev. Mod. Phys. **59**, 1 (1987).
[15] T. Brandes and F. Renzoni, Phys. Rev. Lett. **85**, 4148 (2000).
[16] Yu. A. Pashkin *et al.*, Nature (London) **421**, 823 (2003).